Review Article

Room Temperature Surface Bio-Sulfurisation via Natural *Sativum Annilin* and Bioengineering of Nanostructured CuS/Cu_2S

G. G. Welegergs[1,2,3]
https://orcid.org/0000-0002-7729-4989
getgiday@gmail.com
S. Dube[4]
https://orcid.org/0000-0001-7083-1772
N. Botha[1,2]

Sh. Azizi[1,2]

M. Akbari[1,2]
https://orcid.org/0000-0003-1875-2721
M. G. Tsegay[1,2]
https://orcid.org/0000-0003-2513-5836
Ch. Mtshali[1,2]

F. Ezema[1,2]

A. Gibaud[1,2,7]
https://orcid.org/0000-0002-7777-6427
M. P. Seopela[1,2,9]
https://orcid.org/0000-0002-9680-1763
M. Maaza[1,2]
https://orcid.org/0000-0003-3429-509X
N. Numan[1,2]
https://orcid.org/0000-0003-3341-6961

Z. Nuru[1,2,5]
https://orcid.org/0000-0001-7240-642X
K. Cloete[1,2]
https://orcid.org/0000-0002-7245-7785
I. Madiba[1,2]
https://orcid.org/0000-0002-7091-9202
R. Morad[1,2]
https://orcid.org/0000-0002-1475-0422
H. G. Gebretinsae[1,2]
https://orcid.org/0000-0001-8265-8372
Z. Khumalo[1,2]
https://orcid.org/0000-0002-2124-0498
A. Krief[1,2,6]
https://orcid.org/0000-0002-9223-1644
M. Henini[1,2,8]
https://orcid.org/0000-0001-9414-8492
M. Chaker[1,2,10]
https://orcid.org/0000-0002-4960-7167

1 UNESCO–UNISA Africa Chair in Nanoscience–Nanotechnology, College of Graduate Studies, University of South Africa.
2 Nanosciences African Network iThemba LABS, National Research Foundation, South Africa.
3 Department of Chemistry, Debre Berhan University, Ethiopia.
4 Department of Chemistry, University of South Africa.
5 Department of Physics, Adigrat University, Ethiopia.
6 Department of Chemistry, University of Namur, Belgium.
7 Institute of Molecules and Materials, Le Mans University, France.
8 Department of Physics and Astronomy, University of Nottingham, UK.
9 Department of Chemical Sciences, University of Johannesburg, South Africa.
10 INRS-Energy and Materials, Canada.

Nano-Horizons
https://www.scienceopen.com/collection/NanoHorizons https://doi.org/10.25159/NanoHorizons.45486dad4f94
Volume 2 | 2023 | 27 pages

Abstract

In this contribution, we report, for the first time, on the surface bio-sulfurisation of metallic surfaces at room temperature via natural *sativum annilin*. More precisely, this bio-sulfurisation is validated on bioengineered nanostructured $Cu_{2-X}S$ surfaces using natural organosulfur compounds emitted from *Sativum allium L.* as efficient sulfurisation chemical agents. It is validated that virgin copper surfaces can be sulfurised at room temperature without adding any extra chemical or physical processes. In addition to the validation of the green sulfurisation process of the copper surface, the bioengineered $Cu_{2-X}S$ exhibited a multiscale 1-D tubular morphology with $Cu_{2-X}S$ nanotubules and nanocones. Such a nanostructured $Cu_{2-X}S$ surface exhibited an excessive optical selectivity, a superhydrophobicity response in addition to a remarkable site selective mercury adsorption.

Keywords: surface bioengineering; surface nanostructuring; green/bio-sulfurisation; multifunctionality; copper sulfide; $Cu_{2-X}S$, *Allium sativum L.*

1 Introduction

The copper sulfides family consists of a rich group of chemical compounds of natural or synthetic origin[1]–[13]. Such a family encompasses, among other things, covellite (CuS), yarrowite ($Cu_{1.12}S$), spionkopite ($Cu_{1.39}S$), geerite ($Cu_{1.6}S$), anilite ($Cu_{1.75}S$), digenite ($Cu_{1.80}S$), djurleite ($Cu_{1.96}S$) and chalcocite (Cu_2S) in addition to the villamaninite (CuS_2). This latter phase, synthesised at high pressure, is a degenerate semiconductor with an incomplete p-valence band of sulfur. From a crystallographic viewpoint and as shown in Figure 1, such compounds exhibit a rich set of crystalline structures varying from orthogonal to hexagonal configuration[1]–[13].

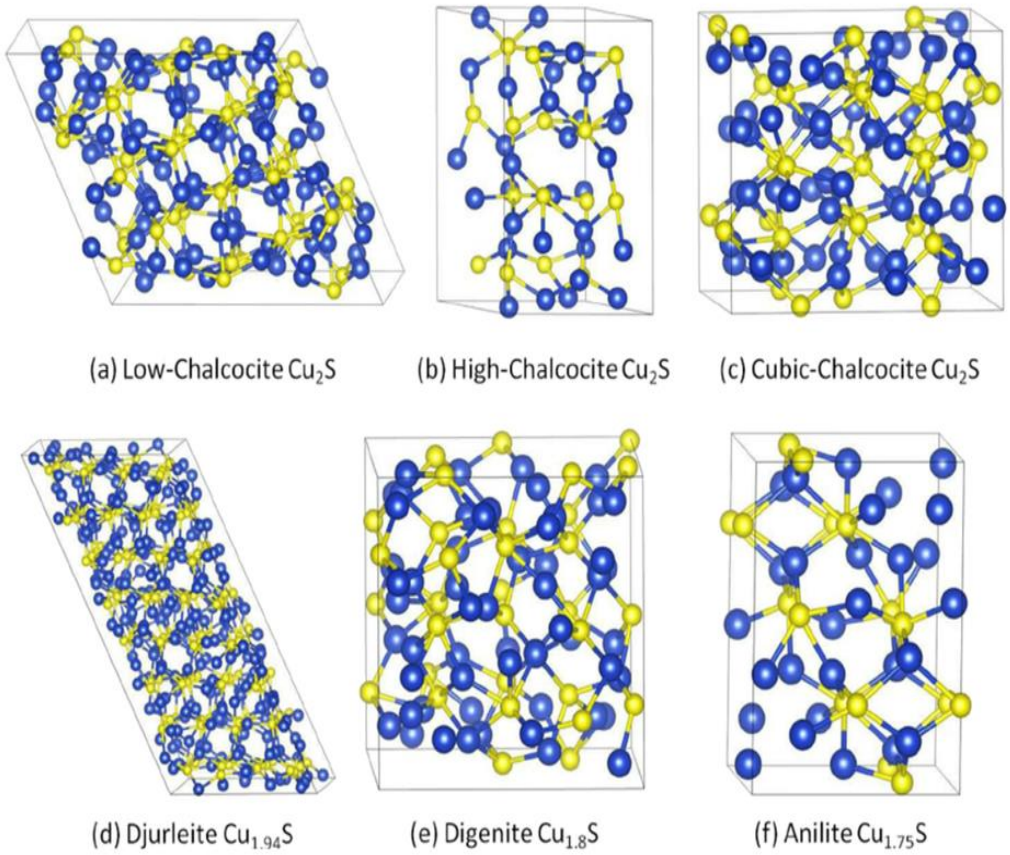

Figure 1: Typical crystallographic structures within the Cu_XS_Y chalcogenide family Such compounds exhibit a rich set of crystalline structures varying from orthogonal to hexagonal configuration

Within such a chalcogenide Cu family and from an electronic viewpoint, the $Cu_{2-X}S$ compounds are p-type semiconductors with several key energy-related technological

applications in solid state solar cells, electroconductive coatings, lithium ion batteries, electrodes, photothermal conversion of solar energy and water splitting[14]–[27].

The above-mentioned properties were found to be enhanced in $Cu_{2-X}S$ exhibiting a net shape anisotropy such as 1-D tubular systems including nanowires, nanorods, nanotubes and nanobelts[28]–[33]. A variety of chemical and physical synthesis routes for well-aligned $Cu_{2-X}S$ 1-D arrays has been developed including hydrothermal growth, template-assisted growth, high-pressure, autoclave processes, chemical vapor deposition, laser-assisted catalytic growth and thermal evaporation. However, these growth methods usually require the use of additional surfactants, catalysts or templates which were found to increase contamination and/or an additional input energy consumption. Likewise, they require an artificial sulfur source including, but not limited to, thiourea (CH_4N_2S, NaS_2O_3, Na_2S), and ammonium sulfate ($(NH_4)_2SO_4$).

Organosulfur compounds in natural systems such as those present in *Allium sativum L.* (known as garlic) could be an effective, green and benign source of sulfur (Table 1). If so, it would allow a green surface sulfurisation process. Hereafter, *Allium sativum L.* would be an ideal source in this regard (Figure 2(a)). Indeed, as presented by Table 1, *Allium sativum L.* contains approximately 33 organosulfur compounds and related complexes (such as alliin, allicin, ajoene, allyl propyl disulfide, diallyl trisulfide, s-allylcysteine, vinyldithiines, and S-allyl mercapto cysteine) with several enzymes (such as alliinase, peroxidases, and myrosinase) and 17 amino acids (such as arginine), in addition to potential doping minerals (Se, Ge, Te and other trace minerals)[34]–[35].

Table 1: Major organosulfur compounds in natural systems such as *Allium sativum*

Chemical compounds found in a single *Allium sativum* bulb	**Formula**	**Concentration (ppm)**	**References**
Alanine	$C_3H_7NO_2$	1 320–31 168	[34]–[35],[58]
Allicin	$C_6H_{10}O\mathbf{S_2}$	1 500–27 800	[34]–[35],[58]
Alliin	$C_6H_{11}NO_3\mathbf{S}$	5 000–10 000	[34]–[35],[58]
Allyl propyl disulfide	$C_6H_{12}\mathbf{S_2}$	36–216	[34]–[35],[58]
Diallyl disulfide	$C_6H_{10}\mathbf{S_2}$	16–613	[34]–[35],[58]
Diallyl sulfide	$C_6H_{10}\mathbf{S_2}$	2–99	[34]–[35],[58]
Diallyl trisulfide	$\mathbf{S}(\mathbf{S}CH_2CH = CH_2)_2$	10–1061	[34]–[35],[58]
Methyl allyl disulfide	$CH_2 = CHCH_2\mathbf{S}CH_3$	6–104	[34]–[35],[58]
Methyl allyl sulfide	$C_4H_8\mathbf{S}$	0.5–4.6	[34]–[35],[58]
Methyl allyl trisulfide	$C_4H_8\mathbf{S_2}$	6–279	[34]–[35],[58]
Methyl propyl disulfide	$C_4H_{10}\mathbf{S_2}$	0.03–0.66	[34]–[35],[58]
S-allyl cysteine	$C_6H_{11}NO_2\mathbf{S}$	10	[34]–[35],[58]

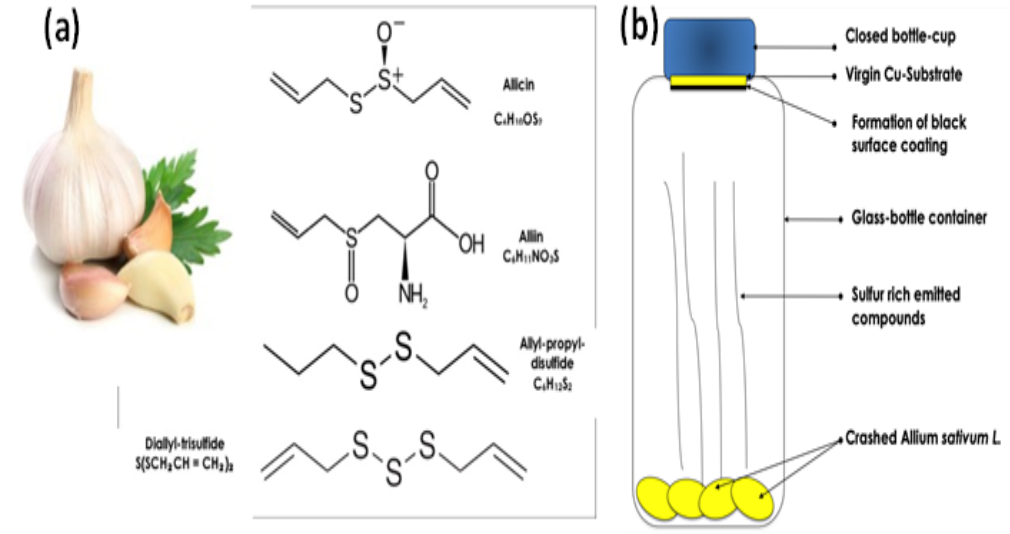

Figure 2: (a) Major organosulfur compounds present in a standard clove of *Allium sativum L.*
(b) Schematic graphical representation of the basic principle of sativation at room temperature

As presented in Table 1, the natural extract of *Allium sativum* contains several sulfur-rich compounds in relatively high concentrations[35]. This, a priori, reinforces the ability of *Allium sativum* as a potential effective green source for surface sulfurisation.

In this contribution, we validate for the first time within the international scientific and technical published literature the possibility of entirely green sulfurisation of Cu surfaces via organosulfur compounds emitted from *Allium sativum L.* This room temperature green sulfurisation approach might be generalised to other metallic surfaces.

The originality of this contribution therefore consists of the following:

(i) The first-time validation of the possibility of sulfurisation of Cu surfaces using natural organosulfur compounds emitted from crashed *Allium sativum L.* at room temperature.

(ii) Such an effective sulfurisation at room temperature is shown to induce not only a sound formation of $Cu_{2-X}S$ but also an additional peculiar nanostructuration of the Cu surface.

(iii) Such a formed nanostructured $Cu_{2-X}S$ exhibited an excessive optical selectivity, a remarkable site selective mercury adsorption in addition to a super hydrophobicity response.

2 Experiments, Results and Discussions

2.1 Synthesis and Methodology

We intended to validate the entire green sulfurisation process of Cu surfaces at room temperature (25°C (293.5 K)) and therefore used the green bioactive volatile organosulfur compounds from garlic (Latin: *Allium sativum L.*) as a natural source of sulfur. In this regard, we used standard garlic cloves from a local market in Stellenbosch (Western Cape, South Africa). Prior to the sulfurisation phase, the copper (Cu, 99.99% in purity) substrates (1.5 cm × 1.5 cm × 0.675 mm) were cleaned ultrasonically with isopropanol, acetone, and thereafter with deionised water for 15 min at each step, and finally dried by blowing N_2 gas. Typically, 50 g of garlic cloves were peeled and chopped using a standard electrical blender. As schematically represented in Figure 2(b), a sticky tape was applied on the back of the Cu substrate to stick it on the cover of the glass container. The distance between the surface of the chopped *Allium sativum L.* and the Cu substrate in the glass container was fixed to ~4 cm. Then the Cu substrates were exposed at various times of 6, 12, 24, 48, 72 and 96 h. Finally, the obtained CuS/Cu_2S coatings onto Cu substrates were air dried. All experiments were performed at room temperature.

2.2 Materials and Characterisation

The scanning electron microscopy (SEM) investigations were conducted on a Verios 5 XHR SEM unit. The UV-VIS-NIR diffuse reflectance studies were acquired using an Ocean Optics unit within the spectral range of 250–1 100 nm. As a standard reference for reflectance measurements, $BaSO_4$ standard was used. With an optical bandgap of ~ 6eV, $BaSO_4$ exhibits a low absorption extending to the UV band correlated to an elevated UV_VIS and NIR reflectance, in addition to its intrinsic phonon resonance at 9 μm. The luminescence measurements were recorded using a fibre-optics linked Ocean Optics system consisting of a UV light-emitting diode source coupled to a high sensitivity QE Pro-FL spectrophotometer. The excitation wavelength was fixed at 240 nm. The XPS measurements were carried out with a VG ESCALAB 220 iXL spectrometer using a monochromatic AI KiX (1486.5 eV) X-ray radiation coupled to a hemispherical analyser at a pass energy of 20 eV.

2.3 Morphological and Size Distribution Investigations

Figure 3(a) displays a typical SEM of the surface of the Cu substrate exposed for 96 h to the organosulfur emission of *Allium sativum* at room temperature. As one can notice, the surface is extensively nanostructured. It looks similar to a field of tubular sea coral reef. More precisely, it consists of major nanotubules with an average internal diameter of about ~271 nm and an average wall thickness of ~83 nm in average at its top end.

Their height is at least ~2.41 µm. In addition to these nanotubes seemingly growing from the Cu substrate surface upwards, there are secondary nanocones growing from the external walls of the nanotubules (Figure 3(b)–(e)). Their shape is conical. Their base diameter is larger than their top one. The population density of such secondary nanocones seems to be dependent on time exposure. As it will be shown later in the section on optical properties, these specific tubular nanostructures are ideal for light trapping and hence optical selectivity and significant hydrophobicity behaviour.

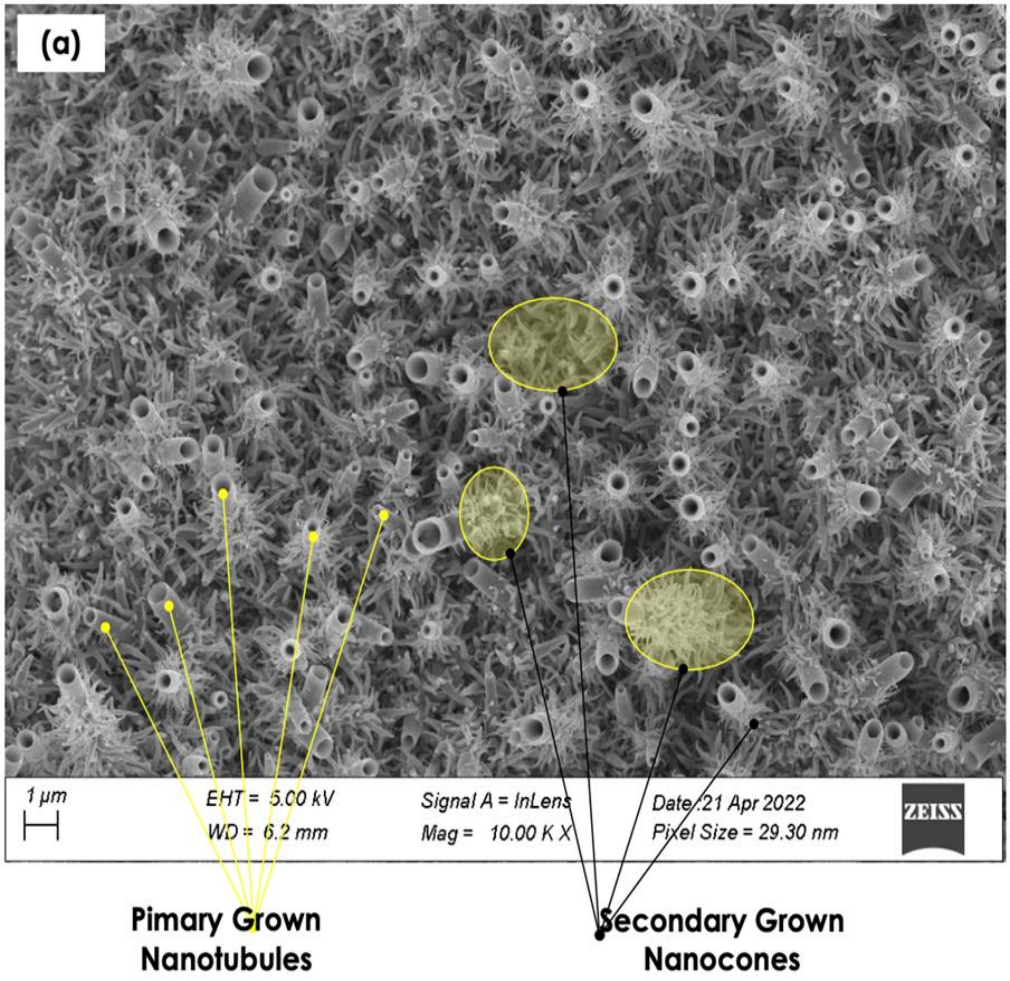

Figure 3: Typical SEM of the surface of the Cu substrate exposed for 96 h to the organosulfur emission of the *Allium* sativum at room temperature
(a) Low magnification
(b–e) High magnification

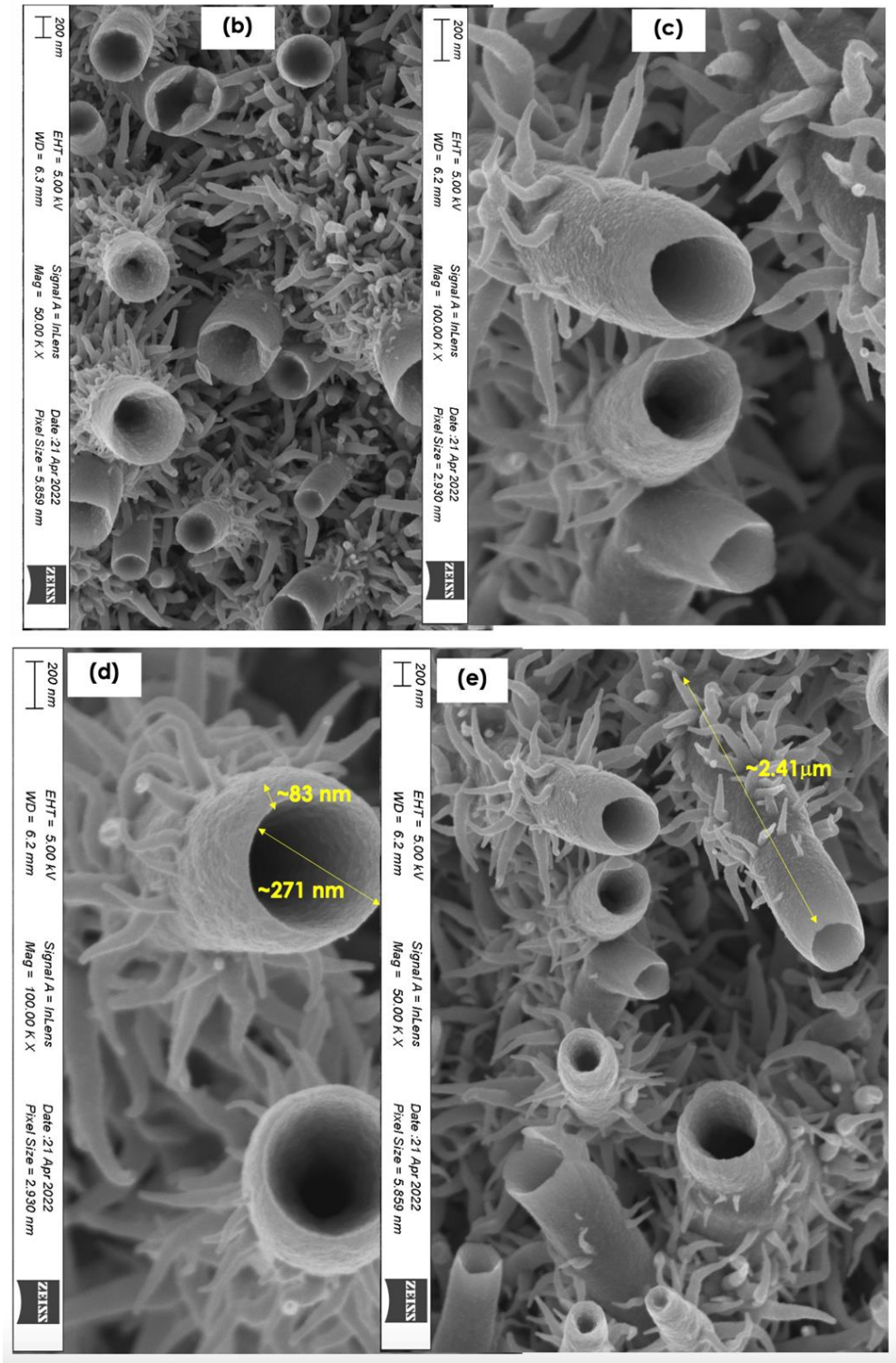
(b)
200 nm
EHT = 5.00 kV
WD = 6.3 mm
Signal A = InLens
Mag = 50.00 K X
Date :21 Apr 2022
Pixel Size = 5.859 nm
ZEISS
(c)
200 nm
EHT = 5.00 kV
WD = 6.2 mm
Signal A = InLens
Mag = 100.00 K X
Date :21 Apr 2022
Pixel Size = 2.930 nm
ZEISS
(d)
~83 nm
~271 nm
200 nm
EHT = 5.00 kV
WD = 6.2 mm
Signal A = InLens
Mag = 100.00 K X
Date :21 Apr 2022
Pixel Size = 2.930 nm
ZEISS
(e)
~2.41µm
200 nm
EHT = 5.00 kV
WD = 6.2 mm
Signal A = InLens
Mag = 50.00 K X
Date :21 Apr 2022
Pixel Size = 5.859 nm
ZEISS

2.4 Chemical and Elemental Analysis

Figure 4(a) shows the various energy dispersive X-ray spectroscopy (EDS) spectra of the various samples exposed at various times of 6, 12, 24, 48, 72 and 96 h to the organosulfur compounds of *Allium sativum*. Yet dominated by Cu peaks, they exhibit an additional S characteristic peak at low energy channels in addition to the oxygen "O" peak at 0.5087 keV and that of carbon "C" at 0.2621 keV. While this carbon originates from the required carbon coating for the SEM studies, the O signal is likely to be associated with the oxidised surface of the Cu substrate. Figure 4(b) singles out the EDS spectra of the samples exposed during the lowest and highest exposure time, ie for 6 h and 96 h respectively. Both are dominated by Cu peaks at various channels located at the vicinity of 0.911, 8.049 and 8.913 keV. The sulfur peak is nearly inexistent for the 6 h whereas it is relatively intense in the case of all samples exposed for 12 h and longer. The corresponding S peak is located at 2.2295 keV. Figure 4(c) displays the ratio of the integrated intensities of S and Cu peaks with the additional corresponding parameters as summarised in Table 2. As one can notice, the ratio S/Cu seems increasing with the exposure time to the organosulfur compounds of *Allium sativum* yet not in a linear manner as one should have expected.

Although these EDS investigations confirm the continuous sulfurisation of the Cu surface, they seem to suggest that the sulfurisation saturates at S/Cu ~1. Likewise, it might be tempting to correlate the obtained phases to the standard stoichiometric $Cu_{2-x}S$ phases; covellite (CuS), yarrowite ($Cu_{1.12}S$), spionkopite ($Cu_{1.39}S$), geerite ($Cu_{1.6}S$), anilite ($Cu_{1.75}S$), digenite ($Cu_{1.80}S$), djurleite ($Cu_{1.96}S$) and chalcocite (Cu_2S). More specifically, one might a priori associate the $Cu_{2-x}S$ exposed during 24 h to spionkopite (Cu/S ~1.37) and that of 72 h and 96 h to covellite (Cu/S ~1). Such a deduction is premature unless supported by additional arguments (for example, crystallographic).

Table 2: EDS deduced relative ratio S/Cu for the exposure time to the organosulfur compounds of *Allium sativum*

Cu integrated intensity	S integrated intensity	Relative ratio S/Cu	Exposure time (hours)	Relative ratio Cu/S
29 468	6 276.7	0.213	6	4.69
62 095	32 434	0.522	12	1.92
90 938.1	66 135	0.727	24	1.37
113 234.8	96 921.4	0.856	48	1.16
131 747.5	120 650.2	0.915	72	1.09
150 311.2	139 469.6	0.927	96	1.07

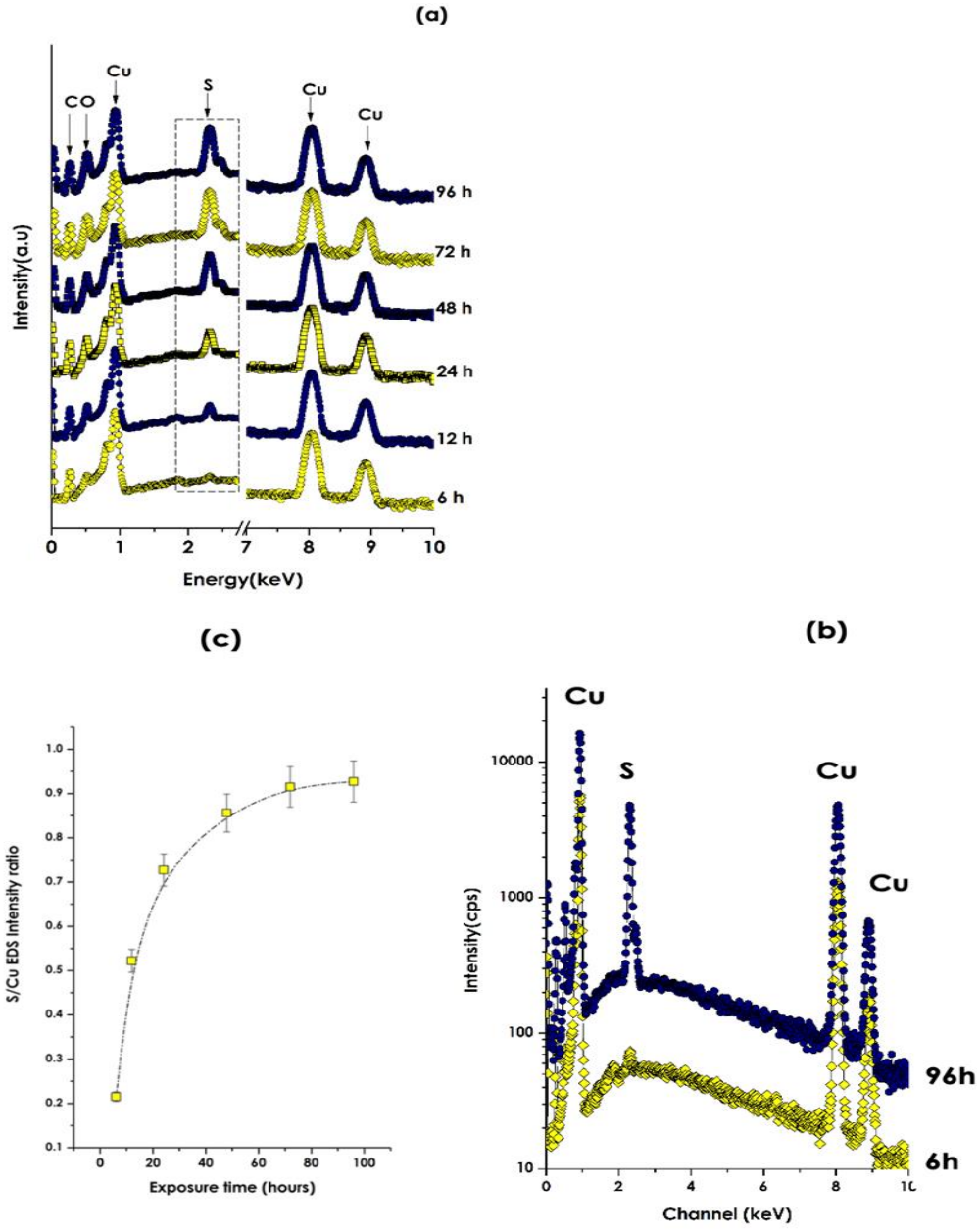

Figure 4: (a) EDS spectra of the various samples exposed at various times of 6, 12, 24, 48, 72 and 96 h to the organosulfur compounds of *Allium sativum*
(b) EDS spectra of the samples sulfurised at 6 h and 96 h
(c) the ratio of the integrated intensities of S and Cu peaks versus the exposure time

2.5 Surface and Interface Investigations

Figure 5 displays a typical X-ray photoelectron spectroscopy (XPS) spectra of the Cu substrate exposed for 96 h to the organosulfur emission of *Allium* sativum at room temperature. Figure 5(a) shows the XPS profile of the Cu 2p. The $Cu2p_{3/2}$ and $Cu2p_{1/2}$ and their satellites are located at the binding energies of 962.84, 954.96, 952.46, 942.96, 934.71 and 932.63 eV respectively. These binding energy values are in agreement with those of standard high purity Cu. Figure 5(b) displays the XPS profile of the S 2p. This consists of the convolution of two major components centred at the energy binding values of 162.68 and 161.73 eV.

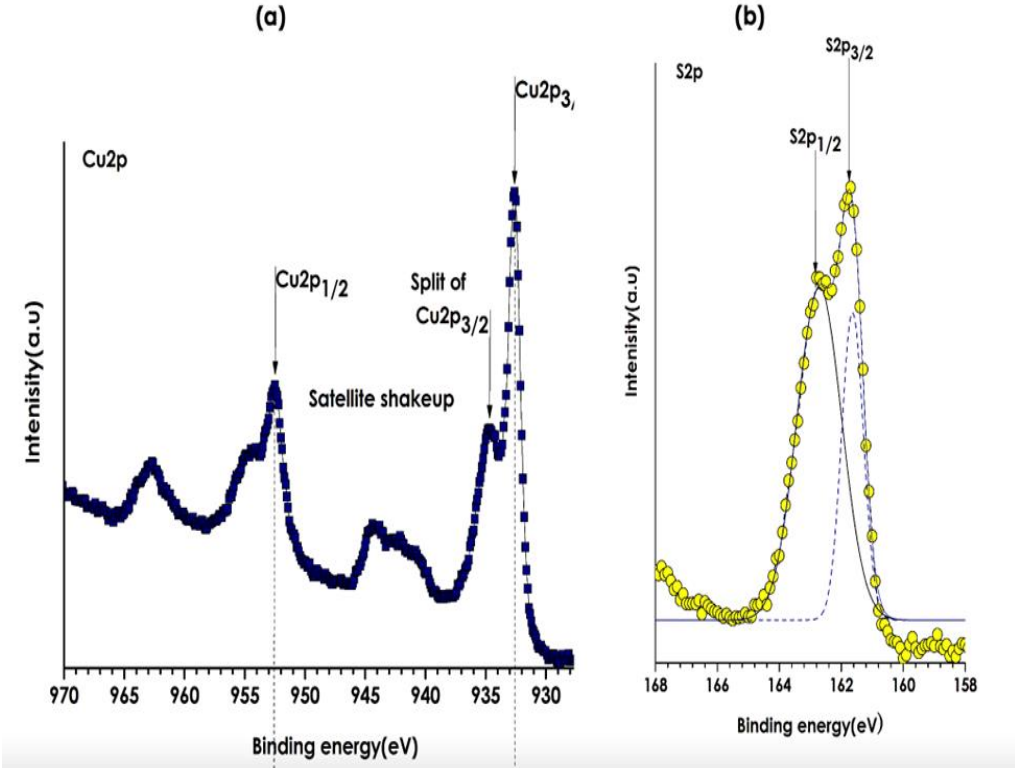

Figure 5: Typical XPS spectra of the Cu substrate exposed for 96 h to the organosulfur emission of *Allium sativum* at room temperature
(a) Profile of the Cu 2p
(b) Profile of the S 2p

The presence of $S2p_{3/2}$ and $S2p_{1/2}$ is in support of a surface sulfurisation of the Cu substrate. In addition, such values are in agreement with those corresponding to covellite as reported by Folmer and Jellinek[36] and Pattrick *et al.*[37]. The covellite phase is represented by the formula Cu3 + (S2)2−S−, where two-thirds of the sulfur atoms form S2 groups while one-third of the sulfur atoms (SB) are isolated. The S $2p_{3/2}$ peak located

close to 161.03 eV corresponds to the isolated sulfur atoms (labelled as planar sulfur) while the peak located close to 161.8 eV corresponds to S2 units (sulfur in S–S bonds). Furthermore, the observed SB 2p3/2 peak position of 161.03 eV is 0.67–0.77 eV lower than that of the chalcocite (161.7 eV). Likewise, one should mention that the XPS at different locations of samples were quasi-similar pointing, a priori, to a homogeneous surface sulfurisation.

As a preliminary conclusion of this subsection, one might safely deduce that the surface sulfurisation took place at room temperature and is homogeneous.

2.6 Crystallographic Studies

Figure 6(a) displays the room temperature X-ray diffraction pattern of the Cu substrate exposed for 96 h to the organosulfur emission of *Allium sativum*. As one can distinguish, there is a set of three categories of peaks. First, three intense Bragg peaks centred at $2\Theta \sim 43.302$, 50.404 and 74.501° respectively. They have been identified and labelled as Cu(111), Cu(200) and Cu(222). Second, a less intense Bragg peak positioned at $2\Theta \sim 36.201°$. This last category has been identified as likely corresponding to the Cu_2O (110) reflection. Third, and in addition to these Cu and Cu_2O Bragg reflections, there is a prominent broad peak extending from $2\Theta \sim 20°$ to about $2\Theta \sim 60°$.

This could be a signature of an amorphous CuS or Cu_2S. It should be mentioned that nearly all Bragg diffraction reflections of crystalline CuS (covellite) or Cu_2S (chalcocite) are located within this angular range of $2\Theta \sim 20–60°$. This includes the (100), (101), (102), (103), (110), (114), and (203) reflections. Within such an angular range, the simulation of the full XRD spectrum requires three sharp Gaussian contributions and one broad Gaussian base component as shown in Figure 6(b). This last broad Gaussian section seems to support the amorphous nature of the $Cu_{2-X}S$ component. If one considers the Scherrer approximation relating the width of the Bragg peaks $\Delta\theta_B$ to the crystals' size $\langle ø \rangle$; ($\langle ø \rangle \sim \lambda / \Delta\theta_B \cos\theta_B$). The average size of the Cu, Cu_2O and amorphous $Cu_{2-X}S$ crystals are 11.4 nm, 8.1 nm and 1.2 nm respectively.

As a preliminary conclusion of this subsection, one might safely deduce that the $Cu_{2-X}S$ tubular surface is likely to be amorphous onto crystalline Cu substrate with a slightly oxidised interlayer at the interface between the $Cu_{2-X}S$ tubules and the Cu substrate. The sulfurised Cu could be CuS (covellite) or Cu_2S (chalcocite).

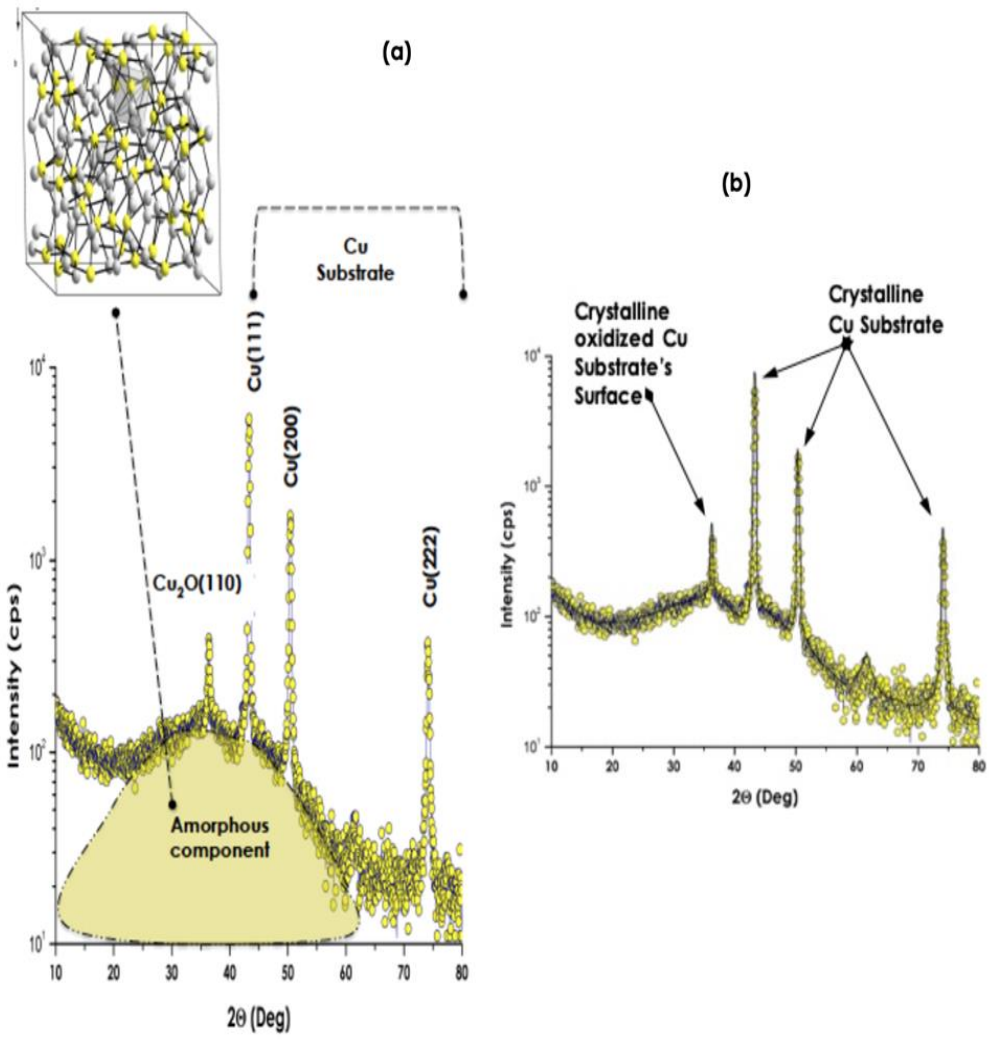

Figure 6: Typical X-ray diffraction pattern of the Cu substrate exposed for 96 h to the organosulfur emission of *Allium* sativum at room temperature
(a) Experimental spectra
(b) With convoluted simulated profiles

2.7 Properties: Superhydrophobicity

As mentioned previously and in relation to the rough nanostructured surface (Figure 1) induced by the green sulfurisation of the Cu substrate s' surface and the formation of the $Cu_{2-X}S$ nanotubules, such a rough surface would likely exhibit a significant hydrophobicity. Figure 7(a) displays the corresponding hydrophobicity testing in the case of a rough surface according to the models of Wenzel[38] and Cassie and

Baxter[39]. The contact angle between the water droplet and the $Cu_{2-X}S$ surface is about 167° in support of an elevated hydrophobicity.

According to Wenzel, and because the liquid does not enter the rough surface (Figure 7(c)), the drop sits on a patchwork of solid surface and air, which leads to contact angles typically between 165° and 175° because the air trapped below the drop "homogenises" the solid. The surface roughness therefore created by the tubular $Cu_{2-X}S$ nanotubules has a considerable influence on the contact angle. An important aspect is the length scale involved. For not-too-rough surfaces, the effect of surface roughness can be ascribed to the so-called Wenzel equation[38]. The equation predicts that if a molecularly hydrophobic surface is rough, the appearance is that of an even more hydrophobic surface. Most solid surfaces are also chemically inhomogeneous and in that regard Cassie and Baxter considered such a case of a smooth but chemically patch heterogeneous surface[39]. In line with Wenzel's model, the $Cu_{2-X}S$ nanostructured Cu surface, the contact angle is about 167° far superior to the wetting contact angle of H_2O onto pure Cu surface(which was found to vary within the range of 60° to 85° as reported by Orlova *et al.*[40]) and schematically presented in Figure 7(b). As a preliminary conclusion of this subsection, one might safely deduce that the $Cu_{2-X}S$ tubular surface is hydrophobic if not superhydrophobic.

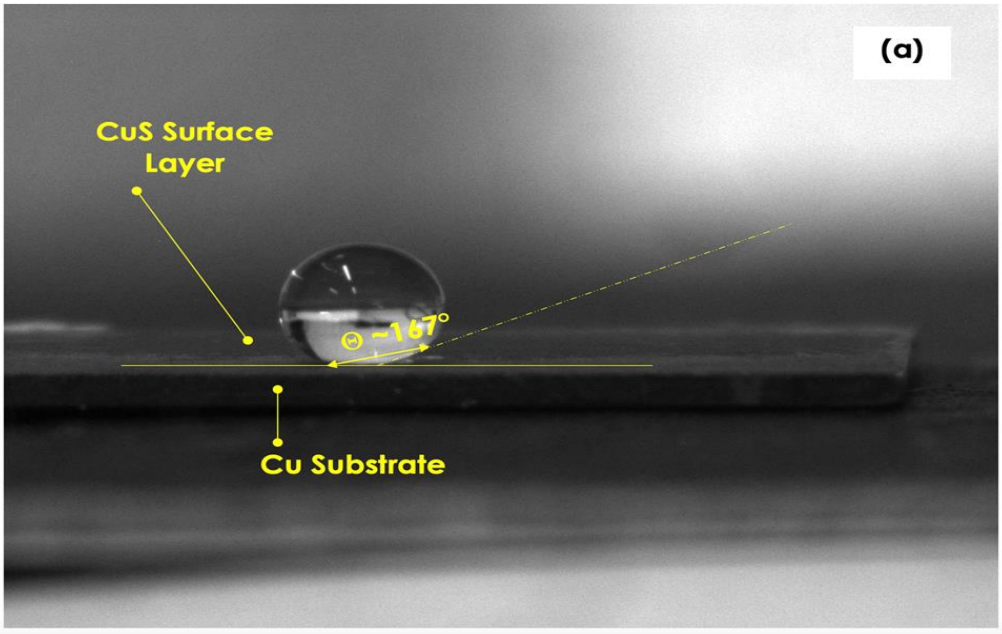

Figure 7: (a) The contact angle experimental test of the Cu substrate exposed for 96 h to the organosulfur emission of *Allium sativum* at room temperature
(b–c) Corresponding to Wenzel and Cassie's model of wettability of a H_2O droplet onto **(a)** a smooth surface and **(b)** and **(c)** a rough surface

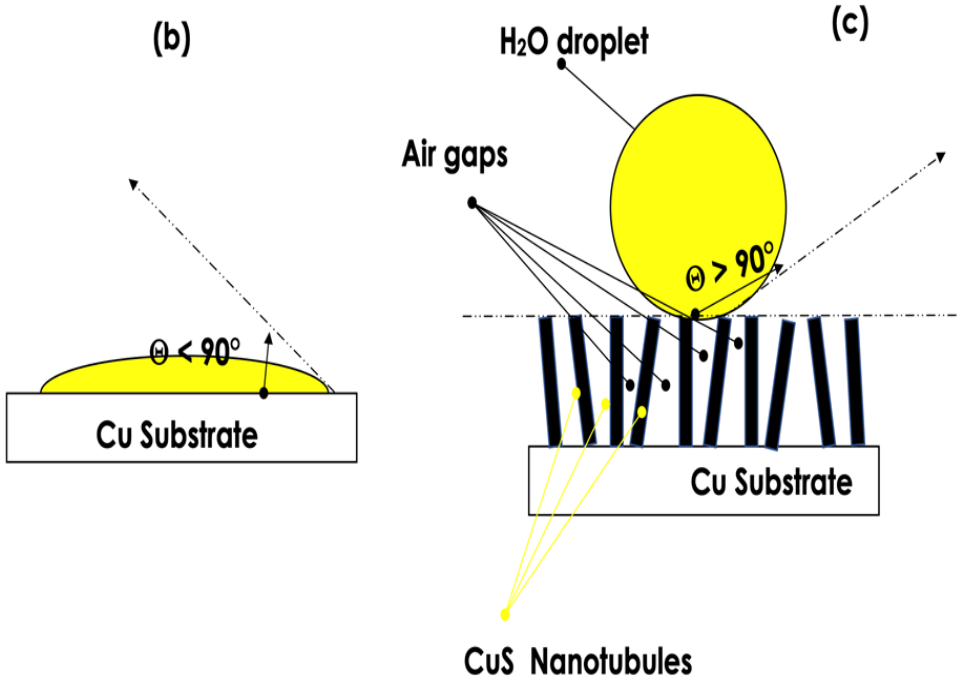

2.8 Properties: Light Trapping and Solar Absorbing Selectivity

Figure 8(a) displays the diffuse reflectance spectra of the Cu substrate exposed at various times of 6, 12, 24, 48, 72 and 96 h to the organosulfur compounds of *Allium sativum L*. One can observe an utmost drop of the reflectivity both in the UV-VIS and NIR-IR spectral regions. Within this latter spectral region of 600–1 100 nm, the reflectivity decreases drastically from 60% to nearly 0% for the samples exposed during 6 and 96 h respectively. Because the optical transmission and reflection are nil for the sample exposed during 96 h to the organosulfur compounds of *Allium sativum L.*, it is safe to conclude on its elevated absorption A ~100% (A + T + R = 100%). In addition to various scattering effects, free-carrier intra-band absorbance[41], generation of mid-gap states and transitions to the conduction band[42], this prominent optical absorption value is likely to be favoured by a light-trapping phenomenon within the various porosity of the $Cu_{2-X}S$ nanotubules as schematically represented in Figure 8(b) and as well established in the field of selective solar absorbers[43]–[45]. In this latter case, it is well stablished that the light trapping in such significantly rough black surfaces is dominated by total reflection and/or multiple scattering phenomena as schematically presented in Figure 8(b)[43]–[46].

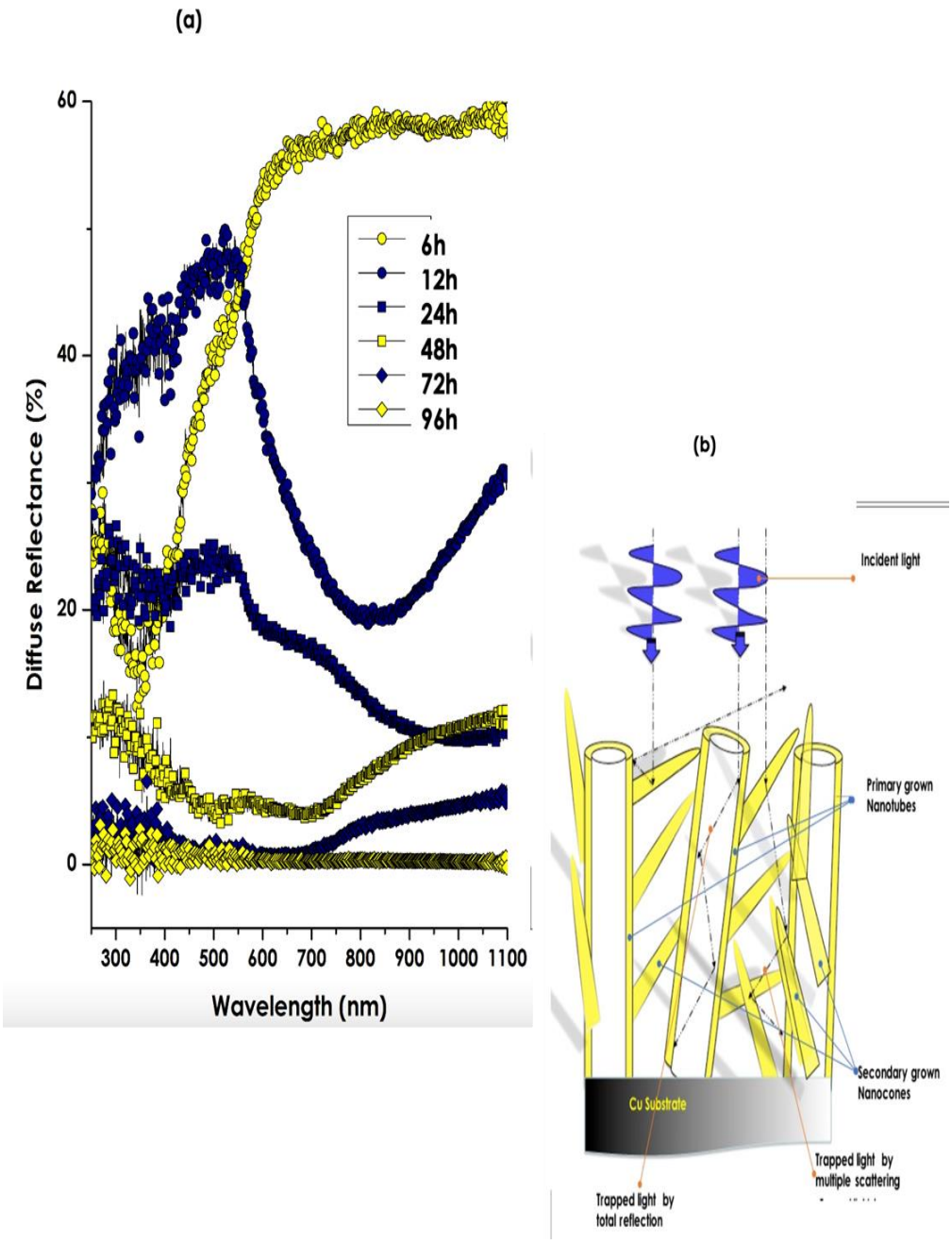

Figure 8: (a) Diffuse reflectance spectra of the Cu substrate exposed at various times of 6, 12, 24, 48, 72 and 96 h to the organosulfur compounds of *Allium sativum L.* **(b)** Proposed model of light trapping at the origin of the paramount decrease of the diffuse reflectivity within the UV-VIS and NIR spectral regions

2.9 Properties: Luminescence Characteristics

Figure 9(a) displays the luminescence spectra of the $Cu_{2-X}S$ samples sulfurised at various times of 6, 12, 24, 48, 72 and 96 h following the exposure to the organosulfur compounds of *Allium sativum L*. All samples exhibit a major emission peaking at about ~507 nm. Although the spectral position of this major emission seems constant, its intensity varies significantly. Smaller is the exposure time, intense is the emission as shown in Figure 9(b). This trend seems to suggest that the emission peaking at 507 nm is caused by a specific identical origin, likely to be defects correlated. Indeed, in the absence of doping, such an emission is likely to be caused by the metallic site deficiencies as in the case of the majority of sulfides[47]–[49]; in this case Cu^{2+}. In line with the effectiveness of nanoscaled $Cu_{2-X}S$ luminescence in the fast growing field of synchronous fluorescence spectroscopy (SFS)[50], it would be sound to explore the possibility of enhancing further the sensitivity by using the luminescence of currently room temperature green, sulfurised Cu substrates as previously demonstrated by Zhang and Wang with CuS nanocubes[51].

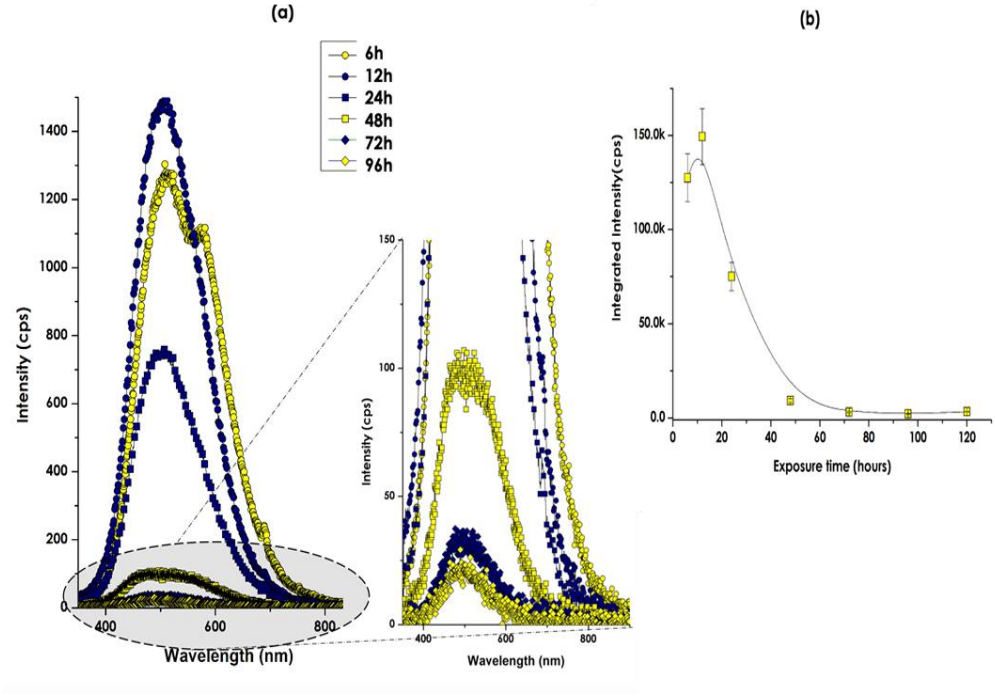

Figure 9: (a) Typical luminescence spectra of the CuS samples sulfurised at various times of 6, 12, 24, 48, 72 and 96 h following the exposure to the organosulfur compounds of *Allium sativum L*.
(b) Variation of the integrated intensity of the major emission peak centred at ~507 nm versus the exposure time

2.10 Properties: Mercury Decontamination in Mining Contaminated Water

In view of the high chemical affinity of Hg with S, we explored the potential of removing Hg in contaminated mining water with the current green sulfurised Cu. In this regard, a standard H_2O solution contaminated with phenyl-mercury acetate $Hg(CH_3COO)_2$ is considered. Figure 10(a) displays the XRD of the Cu substrate exposed for 96 h and immersed within the $Hg(CH_3COO)_2/H_2O$ solution under continuous steering for 15 min. As one can notice, in addition to the various relatively sharp Cu Bragg diffractions centred at 2Θ ~36.3886, 43.2588, 50.4557 and 51.8916° and identified as Cu(111), Cu(200), Cu(220) and Cu(311), there are two additional sharp Bragg diffractions peaks located at 2Θ ~26.3628 and 30.2923°. The latter distinctive diffraction peaks are likely to be correlated to HgS (111) and HgS (200). If so, this would confirm the chemical reaction between the phenyl-mercury acetate and the CuS/Cu_2S nanotubules at room temperature. In addition, there is a moderately broader distinguishable Bragg Peak centred at 28.3233° which was allocated to $Cu_{2-X}S$ (102) Bragg reflection.

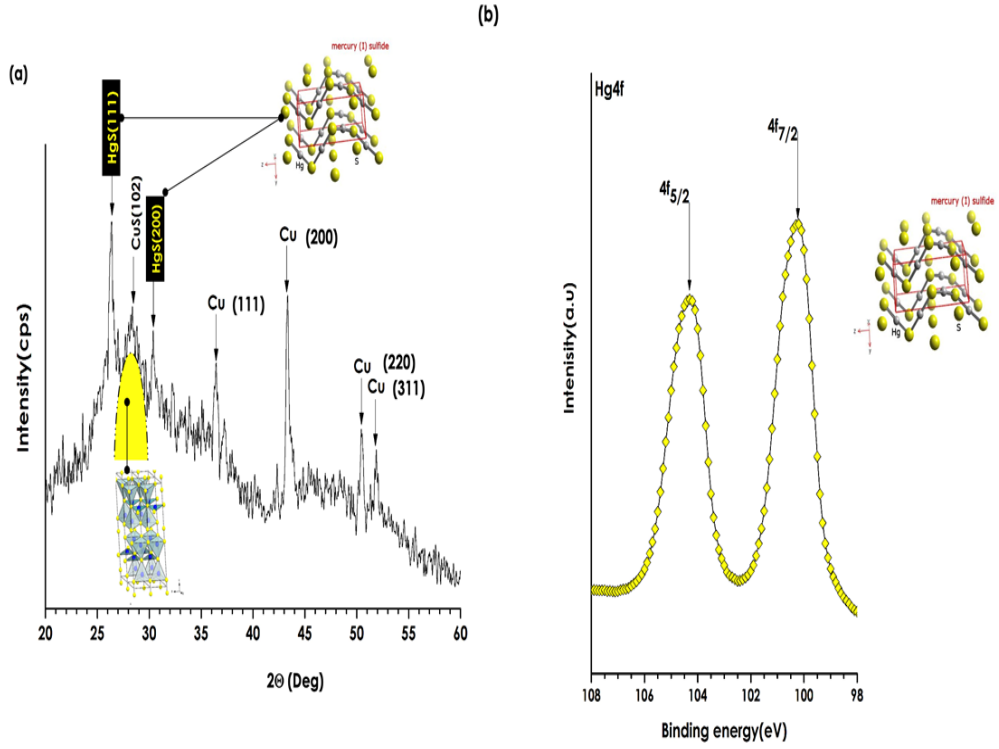

Figure 10: XRD profile of the Cu substrate exposed for 96 h and immersed within the $Hg(CH_3COO)_2/H_2O$ solution under continuous steering for 15 min
(b) Its corresponding XPS spectrum displaying the Hg4f spectrum

To confirm the Hg trapping or its chemisorption at the $Cu_{2-X}S$ surface, XPS studies were conducted on the sample exposed to the $Hg(CH_3COO)_2/H_2O$ solution. Figure 10(b) displays the corresponding XPS spectrum. More precisely, it reports the Hg4f spectrum. As one can notice, this Hg4f spectrum consists of two main distinctive contributions, namely, $Hg4f_{5/2}$ and $Hg4f_{7/2}$ confirming thus the Hg(II) sorption by the $Cu_{2-X}S$ giving, a priori, birth to a surface HgS cinnabar layer onto the CuS nanotubules.

As a preliminary conclusion of this subsection, one might safely deduce there is a net sorption of Hg onto CuS nanotubules inducing the formation of a thin cinnabar HgS layer. The formation of this layer seems to induce a local moderate crystallographic ordering of the CuS with a main crystallographic orientation of (102).

To sustain such a chemisorption of Hg onto the nanostructured CuS surface, computational investigations were performed.

As mentioned previously, the XRD analysis of our experiment indicates a signature of an amorphous CuS. A systematic theoretical study indicates that the most stable surface of CuS is (001) direction with Cu-S and S-S termination[59]. The CuS(001)-Cu/S (S1) and CuS(001)-S-S (S2) surfaces were therefore constructed from the hexagonal bulk CuS with space group P63/mmc with a = b = 3.797 Å and c = 16.441 Å. A four-layer slab with (3*3) unit cell and 12 Å of vacuum in z direction was used to model the surface structure. The position of all atoms except the atoms in the last two bottom layers of the surface were allowed to relax during the structure optimisation[52]. All calculations were performed in the framework of spin-polarised density functional theory (DFT) using the Perdew-Burke-Enzerhoff generalised gradient approximation (GGA-PBE) exchange–correlation functional applied in the Quantum-Espresso package[53]. The first Brillouin zone was modelled by a Monkhorst-Pack scheme grid of gamma point only[54].

The adsorption of elemental mercury (Hg^0) and mercury acetate ($C_2H_3HgO_2$) on two CuS(001) surfaces were studied and the adsorption energy is calculated by the following expression:

$$E_{ads} = {}_{ECuS\text{-}mercury} - E_{CuS} - E_{mercury}$$

where ${}_{ECuS\text{-}mercury}$, E_{CuS}, and $E_{mercury}$ are the total energy of adsorbate Hg/surface, the total energy of surface and the total energy of isolated mercury species.

The dispersion interaction was applied via Grimme DFT-D3 corrections[55]–[56]. Three different sites, top of S atom (S site), top of Cu atom (Cu site), and in the middle of S atoms (M site) for CuS(001)-Cu/S surface and two different sites, top of S atom (S site), and in the middle of S atoms (M site) for CuS(001)-S-S surface were considered. The optimised structures of Hg atom adsorbed on surface are shown in Figure 11(a). The adsorption energies with and without dispersion interaction are presented in Table 3. The interaction between the mercury atom and the CuS(001) surface is mostly

the dispersion interaction indicating the weak adsorption of elemental Hg on CuS surface. Our results also demonstrate that the middle site (between S atoms on the surface) is the most favourable site in both surface terminations. Also, the interaction of mercury with S atoms is roughly twice stronger than its interaction with Cu atom.

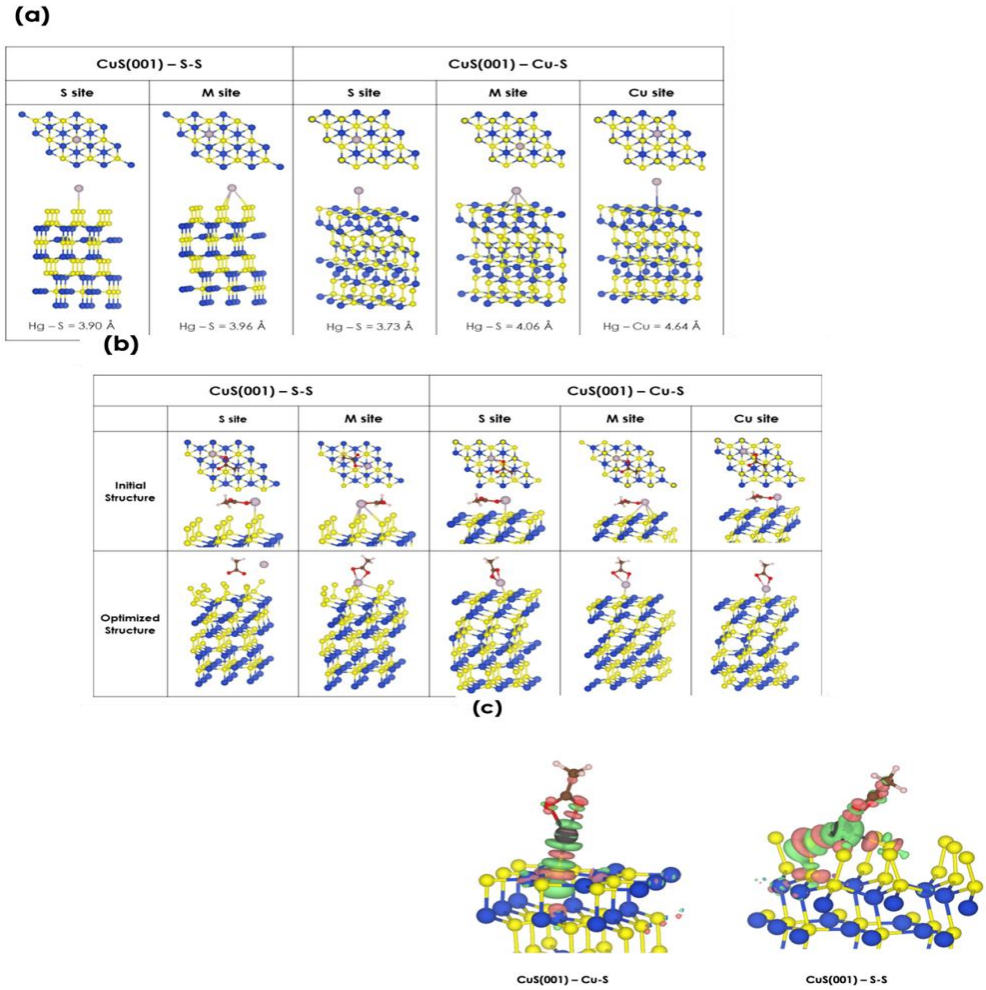

Figure 11: (a) The optimised structure of adsorbed elemental Hg on CuS(001)-Cu-S and CuS(001)-S-S surfaces. The smallest Hg bond with the surface is shown for each structure

(b) The initial and optimised structure of adsorbed Hg-Acetate on CuS(001)-Cu-S and CuS(001)-S-S surfaces

(c) The charge density difference of Hg-Acetate adsorbed on CuS(001)-Cu-S and CuS(001)-S-S surfaces. The green and pink colours mean the negative and positive values corresponding to the loss and gain of electrons. The ISO value sets at 0.0025 e/a.u.^{3}

Table 3: The adsorption energies of elemental Hg and Hg-acetate on CuS(001) surface with two different terminations with and without Van der Waals interaction

E_{ads} (eV)		CuS(001) – S-S		CuS(001) – Cu-S		
		S site	M site	S site	M site	Cu site
Hg^0	without D3	−0.025	−0.036	−0.038	−0.024	−0.010
	including D3	−0.1508	−0.217	−0.185	0.254	−0.115
$(C_2H_3HgO_2)$	without D3	−1.86	−2.169	−1.330	−1.620	−1.538
	including D3	−2.211	−2.616	−1.761	−1.990	−1.914

2.11 Hg-Acetate Adsorption on CuS(001) Surface

The same adsorption sites as those in the previous section were considered to study the interaction of Hg-acetate with CuS(001) surface. The initial and optimised structures are shown in Figure 11(b). In the case of CuS(001)-Cu-S surface, the Hg-acetate interacts strongly with the closest S atom on the surface from mercury side with relatively strong interaction energy compared to the elemental mercury. The highest interaction energy is 1.62 eV which increases to 1.99 eV by considering the dispersion interaction. Less than 20% of the total interaction is therefore dispersion energy whereas almost 90% of the interaction of elemental mercury with surface was dispersion energy. $(C_2H_3HgO_2)$ interacts more strongly with S-S terminated surface with interaction energy of −2.616 eV including the dispersion energy. In order to see the involved interacting atoms, the charge density difference of adsorbed Hg-acetate on the middle site of Cu(001)-Cu-S and Cu(001)-S-S surface are plotted in Figure 11(c). The green and pink colours indicate the negative and positive values corresponding to the loss and gain of electrons. The ISO value sets at 0.0025 e/a.u.^{3}.

In general, our results indicate that the $(C_2H_3HgO_2)$ has a strong chemisorption on the CuS(001) surfaces in which dissociation of $(C_2H_3HgO_2)$ can take place. The CuS surface can therefore be used to adsorb mercury.

Lastly, and as a follow up of this study, the same approach has been applied successfully on other metallic surfaces. Likewise, it is being applied on thin films of Cu deposited onto standard substrates including glass and silicon. Size effects in general[57] and their super capacity storage properties in particular[58].

3 Conclusions

In this contribution, we validated the possibility of green surface sulfurisation at room temperature of copper by using organosulfur compounds derived from *Allium sativum L.* as an effective green source of sulfur. The sulfurised Cu surface exhibited a nanostructured tubular 1-D morphology. More precisely, it consisted of main prime grown CuS or Cu_2S nanotubules with secondary grown nanocones. Their population

density was found to be dependent on exposure time. The various crystallographic, elemental, surface–interface investigations seem to indicate that the CuS/Cu_2S part was amorphous. Also, it was shown that such a bioengineered 1-D nanostructured CuS/Cu_2S exhibits a superhydrophobicity combined to a remarkable solar light optical selectivity. In addition, such a bioengineered nanostructured CuS/Cu_2S displayed a noteworthy chemical affinity to mercury contaminants in H_2O. As a future study, it is intended to (i) identify the exact mechanism of sulfurisation via the organosulfur compounds derived from *Allium sativum L*., and (ii) identify the exact nature of the sulfurised Cu phase, ie its covellite (CuS) or chalcocite (Cu_2S) nature. Furthermore, the sulfurisation at room temperature of other metallic surfaces would be explored.

4 Acknowledgements

We are grateful to the following supporting institutions: the University of South Africa, iThemba LABS, the National Research Foundation of South Africa, the African Laser Centre, the international Organization for Women in Science for the Developing World, the Abdus Salam International Centre for Theoretical Physics, the Royal Society-London, the United Nations Educational, Scientific and Cultural Organization, the French Foreign Ministry and the ADESFA (support for the development of French higher education in Africa) programme, and the Centre for High Performance Computing in South Africa.

5 Availability of Data and Materials

The data sets used and/or analysed during the current study are available from the corresponding author on request.

6 References

[1] L. S. Whiteside and R. J. Goble, “Structural and compositional changes in copper sulfide during leaching and dissolution,” *Can. Mineral*., vol. 24, no. 2, pp. 247–258, 1986.

[2] A. F. Wells, *Structural Inorganic Chemistry*. 5th ed. Oxford Science Publications, 1984.

[3] R. J. Goble, “Copper sulfides from Alberta; yarrowite Cu9S8 and spionkopite Cu39S28,” *Can. Mineral*., vol. 18, no. 4, pp. 511–518, 1980.

[4] R. J. Goble and G. Robinson, “Geerite, Cu1.60S, a new copper sulfide from Dekalb Township, New York,” *Can. Mineral.*, vol. 18, no. 4, pp. 519–523, 1980.

[5] G. Zhenzhen *et al*., “Super-hydrophobic copper sulfide films as light absorbers for efficient solar steam generation under one sun illumination,” *Semicond. Sci. Technol.*, pp. 1361–6641, 2017.

[6] C. Chan *et al.*, "High-performance lithium battery anodes using CuS nanowires," *Nat. Nanotechnol.*, vol. 3, pp. 31–35, 2008, doi: 10.1038/nnano.2007.411.

[7] R. W. Potter, "An electrochemical investigation of the system copper–sulfur." *Econ. Geol.*, vol. 72, no. 8, p. 1524, 1977, doi: 10.2113/gsecongeo.72.8.1524.

[8] H. T. Evans, "The crystal structures of low chalcocite and djurleite," *Z. Kristallogr.*, vol. 150, pp. 299–320, 1979.

[9] G. Will, E. Hinze, and A. R. M. Abdelrahman, "Crystal structure analysis and refinement of digenite, Cu1.8S, in the temperature range 20 to 500 C under controlled sulfur partial pressure," *Eur. J. Mineral.*, vol. 14, no. 3, pp. 591–598, 2002, doi: 10.1127/0935-1221/2002/0014-0591.

[10] K. Koto and N. Morimoto, "The crystal structure of anilite," *Acta Cryst.*, vol. B26, pp. 915–924, 1970, doi: 10.1107/S0567740870003370.

[11] F. Grønvold and E. F. Westrum, "Thermodynamics of copper sulfides I. Heat capacity and thermodynamic properties of copper(I) sulfide, Cu_2S, from 5 to 950 K," *J. Chem. Thermodyn.*, vol. 19, no. 11, pp. 1183–1198, 1987, doi: 10.1016/0021-9614(87)90056-5.

[12] H. T. Evans, "Crystal structure of low chalcocite," *Nat. Phys. Sci.*, vol. 232, pp. 69–70, 1971, doi: 10.1038/physci232069a0.

[13] M. J. Buerger and B. J. Wuensch, "Distribution of atoms in high chalcocite, Cu_2S," *Sci.*, vol. 141, no. 3577, pp. 276–277, 1963, doi: 10.1126/science.141.3577.276.

[14] C. H. Chen-Ho Lai *et al*., "Direct growth of high-rate capability and high capacity copper sulfide nanowire array cathodes for lithium-ion batteries," *J. Mater. Chem.*, vol. 20, pp. 6638–6645, 2010, doi: 10.1039/c0jm00434k.

[15] Y. Wu, C. Wadia, W. L. Ma, B. Sadtler and A. P. Alivisatos, "Hybrid solar cells with prescribed nanoscale morphologies based on hyperbranched semiconductor nanocrystals," *Nano Lett.*, vol. 8, p. 2551, 2008.

[16] A. B. F. Martinson, J. W. Elam and M. J. Pellin, "Atomic layer deposition of Cu_2S for future application in photovoltaics," *Appl. Phys. Lett.*, vol. 94, p. 123107, 2009, doi: 10.1063/1.3094131.

[17] S. C. Liufu, L. D. Chen, Q. Yao and F. Q. Huang, "Boosting the stable Na storage performance in 1D oxysulfide," *Adv. Energy Mater.*, vol. 9, no. 20, 2019, doi: 10.1002/aenm.201900170.

[18] K. Sun *et al.*, "Operando multi-modal synchrotron investigation for structural and chemical evolution of cupric sulfide (CuS) additive in Li-S battery," *Sci. Rep.*, vol. 7, p. 12976, 2017, doi: 10.1038/s41598-017-12738-0.

[19] M. Basu, *et al.*, "Construction of CuS/Au heterostructure through a simple photoreduction route for enhanced electrochemical hydrogen evolution and photocatalysis," *Sci. Rep.*, vol. 6, p. 34738, 2016, doi: 10.1038/srep34738.

[20] K. V. Kravchyk *et al.*, "Copper sulfide nanoparticles as high-performance cathode materials for Mg-ion batteries," *Sci. Rep.*, vol. 9, p. 7988, 2019, doi: 10.1038/s41598-019-43639-z.

[21] D-F. Zhang, H. Zhang, Y. Shang and L. Guo, "Stoichiometry-controlled fabrication of Cu_xS hollow structures with Cu_2O as sacrificial templates," *Cryst. Growth Des.*, vol. 1, no. 9, pp. 3748–3753, 2011, doi: 10.1021/cg101283w.

[22] C. S. Kim, S. H. Choi and H. H. Bang. "New insight into copper sulfide electrocatalysts for quantum dot-sensitized solar cells: Composition-dependent electrocatalytic activity and stability," *ACS Appl. Mater. Interfaces*, vol. 6, pp. 22078–22087, 2014, doi: 10.1021/am505473d.

[23] S. Couve, L. Gouskov, L. Szepessy, J. Vedel and E. Castel. "Resistivity and optical transmission of Cu_xS layers as a function of composition," *Thin Solid Films*, vol. 15, no. 2, pp. 223–231, 1973, doi: 10.1016/0040-6090(73)90046-1.

[24] Y. Zhao, H. Pan, Y. Lou, X. Qiu, J. Zhu and C. Burda, "Plasmonic $Cu_{2-x}S$ nanocrystals: Optical and structural properties of copper-deficient copper(I) sulfides," *J. Am. Chem. Soc.*, vol. 131, no. 12, pp. 4253–4261, 2009, doi: 10.1021/ja805655b.

[25] J. M. Luther, P. K. Jain, T. Ewers and A. P. Alivisatos, "Localized surface plasmon resonances arising from free carriers in doped quantum dots," *Nat. Mater.*, vol. 10, pp. 361–366, 2011, doi: 10.1038/nmat3004.

[26] L. Fan, R. Ma, Y. Yang, S. Chen and B. Lu, "Covalent sulfur for advanced room temperature sodium-sulfur batteries," *Nano Energy*, vol. 28, pp. 304–310, 2016, doi: 10.1016/j.nanoen.2016.08.056.

[27] N. R. Kim *et al.*, "Conversion reaction of copper sulfide based nanohybrids for sodium-ion batteries," *ACS Sustain. Chem. Eng.*, vol. 5, pp. 9802–9808, 2017, doi: 10.1021/acssuschemeng.7b01692.

[28] X. Zhang, G. Wang, A. Gu, Y. Wei and B. Fang, "CuS nanotubes for ultrasensitive nonenzymatic glucose sensors," *Chem. Commun.*, vol. 45, pp. 5945–5947, 2008, doi: 10.1039/b814725f.

[29] W. Du, X. Qian, X. Ma, Q. Gong, H. Cao and J. Yin. "Shape-controlled synthesis and self-assembly of hexagonal covellite (CuS) nanoplatelets," *Chem.*, vol. 13, no. 11, pp. 3241–3247, 2007, doi: 10.1002/chem.200601368.

[30] X. Rui, H. Tan and Q. Yan, "Nanostructured metal sulfides for energy storage. *Nanoscale*, vol. 6, no. 17, pp. 9889–9924, 2014, doi: 10.1039/C4NR03057E.

[31] P. Roy and S. K. Srivastava, “Nanostructured copper sulfides: Synthesis, properties and applications,” *CrystEngComm*, vol. 17, no. 41, pp. 7801–7815, 2015, doi: 10.1039/C5CE01304F.

[32] K. B. Tang, D. Chen, Y. F. Liu, G. Z. Shen, H. G. Zheng and Y. T. Qian, “Shape-controlled synthesis of copper sulfide nanocrystals via a soft solution route,” *J. Cryst. Growth*, vol. 263, no. 1–4, pp. 232–236, 2004, doi: 10.1016/j.jcrysgro.2003.11.045.

[33] Q. Y. Lu, F. Gao and F. Y. Zhao, “One-step synthesis and assembly of copper sulfide nanoparticles to nanowires, nanotubes, and nanovesicles by a simple organic amine-assisted hydrothermal process,” *Nano Lett.*, vol. 2, no. 7, pp. 725–728, 2002, doi: 10.1021/nl025551x.

[34] S. H. Omar and N. A. Al-Wabel, “Organosulfur compounds and possible mechanism of garlic in cancer,” *Saudi Pharm. J.*, vol. 18, pp. 51–58, 2010, doi: 10.1016/j.jsps.2009.12.007.

[35] C. A. Newall, L. A. Anderson and J. D. Phillipson, *Herbal Medicines: A Guide for Health-Care Professionals*. London: Pharmaceutical Press, 1996.

[36] J. C. W. Folmer and F. Jellinek, “Structural and electronic instabilities of transition metal chalcogenides,” *J. Less Common Met.*, vol. 76, no. 1–2, pp. 153–162, 1980, doi: 10.1016/0022-5088(80)90019-3.

[37] R. A. D. Pattrick *et al.*, “The structure of amorphous copper sulfide precipitates: An X-ray absorption study,” *J. Geochim. Cosmochim. Acta*., vol. 61, no. 10, pp. 2023–2036, 1997, doi: 10.1016/S0016-7037(97)00061-6.

[38] R. N. Wenzel, “Resistance of solid surfaces to wetting by water,” *Ind. Eng. Chem.*, vol. 28, no. 8, pp. 988–994, 1936, doi: 10.1021/ie50320a024.

[39] A. B. D. Cassie and S. Baxter, “Wettability of porous surfaces,” *Trans. Faraday Soc.*, vol. 400, p. 546, 1944, doi: 10.1039/tf9444000546.

[40] E. Orlova D. Feoktistov and G. Kuznetzov, “Investigation of drop dynamic contact angle on copper surface,” *EPJ Web of Conferences*, vol. 82, p. 01053, 2015, doi: 10.1051/epjconf/20158201053.

[41] J. Liu and D. Xue, “Rapid and scalable route to CuS biosensors,” *J. Mater. Chem.*, vol. 21, p. 223, 2011, doi: 10.1039/C0JM01714K.

[42] C. Ratanatawanate and A. Bui, “Rapid and scalable route to CuS biosensors,” *J. Phys. Chem.*, vol. 115, p. 6175, 2011.

[43] M. Maaza, B. D. Ngom, Z. Y. Nuru and S. Khamlich, “Surface–interface investigation and stability of cermet-based solar absorbers by grazing angle X-rays reflectometry: Pt-Al2O3 case,” *Arab. J. Sci. Eng.*, vol. 39, no. 7, pp. 5825–5846, 2014, doi: 10.1007/s13369-014-1110-y.

[44] L. Kotsedi *et al.*, "Femtosecond laser surface structuring of molybdenum thin films," *Appl. Surf. Sci.*, vol. 353, pp. 1334–1341, 2015, doi: 10.1016/j.apsusc.2015.08.047.

[45] A. Karoro *et al.*, "Laser nanostructured Co nanocylinders-Al 2 O 3 cermets for enhanced & flexible solar selective absorbers applications," *Appl. Surf. Sci.*, vol. 347, pp. 679–684, 2015, doi: 10.1016/j.apsusc.2015.04.098.

[46] T. Siby, H. Owen and M. A. Zaeem, "Unveiling the role of atomic defects on the electronic, mechanical and elemental diffusion properties in CuS," *Scripta Materialia* vol. 192, pp. 94–99, 2021, doi: 10.1016/j.scriptamat.2020.10.012.

[47] M. I. Zakirov *et al.*, "Spectral-kinetic characteristics of ZnS phosphors obtained using the method of vapor transport synthesis in a closed system," *J. Appl. Spectrosc.*, vol. 82, p. 947, 2016, doi: 10.1007/s10812-016-0210-8.

[48] P. F. Smet, I. Moreels, H. Hens and D. Poelman, "Luminescence in sulfides: A rich history and a bright future," *Mater.*, vol. 3, pp. 2834–2883, 2010, doi: 10.3390/ma3042834.

[49] K. Ren *et al.*, Localized defects on copper sulfide surface for enhanced plasmon resonance and water splitting," *Small.*, vol. 13, p. 1700867, 2017, doi: 10.1002/smll.201700867.

[50] L. Wang, A. N. Liang, H. Q. Chen, Y. Liu, B. B. Qian and J. Fu, "Ultrasensitive determination of silver ion based on synchronous fluorescence spectroscopy with nanoparticles," *Anal. Chim. Acta*, vol. 616, p. 170, 2008, doi: 10.1016/j.aca.2008.04.027.

[51] J. B. F. Lloyd, "Synchronized excitation of fluorescence emission spectra," *Nature*, vol. 231, p. 64, 1971, doi: 10.1038/physci231064a0.

[52] Z. Xiaojun and G. Wang, "Luminescent CuS nanotubes as silver ion probes," *Spectrochimica Acta Part A*, vol. 72, pp. 1071–1075, 2009, doi: 10.1016/j.saa.2008.12.038.

[53] Á. Morales-García, J. He, A. L. Soares and H. A. Duarte, "Surfaces and morphologies of covellite (CuS) nanoparticles by means of ab initio atomistic thermodynamics," *CrystEngComm*, vol. 19, no. 22, pp. 3078–3084, 2017, doi: 10.1039/C7CE00203C.

[54] P. Perdew, K. Burke and M. Ernzerhof, "Generalized gradient approximation made simple," *Phys. Rev. Lett.* vol. 77, p. 3865, 1996, doi: 10.1103/PhysRevLett.77.3865.

[55] S. Scandolo, P. Giannozzi, C. Cavazzoni, S. de Gironcoli, A. Pasquarello and S. Baroni, "First-principles codes for computational crystallography in the Quantum-ESPRESSO package," *Z. Kristallogr.*, vol. 220, p. 574, 2005, doi: 10.1524/zkri.220.5.574.65062.

[56] H. J. Monkhorst and J. D. Pack, "Special points for Brillouin-zone integrations," *Phys. Rev. B*, vol. 13, p. 5188, 1976, doi: 10.1103/PhysRevB.13.5188.

[57] S. Grimme, J. Antony, S. Ehrlich and H. Krieg, “A consistent and accurate ab initio parametrization of density functional dispersion correction (DFT-D) for the 94 elements,” *J. Chem. Phys.*, vol. 132, p. 154104, 2010, doi: 10.1063/1.3382344.

[58] C. C. Patiño-Morales et al., “Antitumor effects of natural compounds derived from *Allium sativum* on neuroblastoma: An overview,” *Antioxidants*, vol. 11, no. 1, p. 48, 2022, doi: 10.3390/antiox11010048.